Outdoor Sound Propagation Modelling in Complex Environments: Recent Developments in the Parabolic Equation Method

Philippe Blanc-Benon
Ecole Centrale de Lyon
Centre acoustique
LMFA UMR CNRS 5509
36 Avenue Guy de Collongue
69134 ECULLY Cedex France

philippe.blanc-benon@ec-lyon.fr

ABSTRACT

In complex environments the modelling of outdoor sound propagation implies to take into account the mixed influence of ground characteristics (topography, obstacles, impedance, etc.) and atmospheric conditions (refraction and turbulence). During the last decade significant progress has been made in the modelling of sound propagation over distances ranging from hundreds meters to kilometres, and the agreement between calculated and measured fields has been greatly improved. New developments appear in the parabolic-equation method. In this paper we present a method which evaluates the propagation of an acoustic wave above uneven terrains including realistic meteorological parameters. In our approach the effects of the topography are modelled using appropriate rotated co-ordinates systems in order to treat the non-flat ground as a succession of flat domains. We also examine the influence of scale resolution on numerical simulation of long range sound propagation through the turbulent atmosphere. Currently, we generate the turbulence using a Random Fourier Modes technique, such that the turbulent fluctuation at any point in the medium (either scalar or vectorial in nature) is calculated from the sum of a chosen number of modes. Our model of outdoors sound propagation is validated both with classical numerical benchmark cases and recent outdoor experiments.

1.0 INTRODUCTION

In complex environments the modelling of outdoor sound propagation implies to take into account the mixed influence of ground characteristics (topography, obstacles, impedance, etc.) and atmospheric conditions (refraction and turbulence). These phenomena have been studied in the literature ([1]). Sound waves are influenced by two principal characteristics: the sound speed (celerity) of the medium, and the velocity of the medium. For numerical simulations of outdoors sound propagation, parabolic equations have been derived using the approximation of the effective sound speed. In this conventional approach the real moving atmosphere is replaced by a hypothetical motionless medium with the effective sound speed $c_{eff} = c + v_x$ where v_x is the wind velocity component along the direction of propagation between source and receiver. When the source and receiver are close to the ground, the preferred direction of sound propagation is nearly horizontal, and standard parabolic equations can be used to predict sound pressure levels. However, in many problems of atmospheric acoustics, refracted sound waves and those scattered by turbulence propagate in directions which may significantly differ from the horizontal axis. A rigorous way to incorporate the effects of a velocity field is to begin with the fundamental equations of fluid mechanics and derive a wave equation which includes the velocity. In the limits of linear acoustic theory, such a wave equation can be derived as the sum of a d'Alembertian operator and additional terms depending on the nature of the velocity field. From such a wave equation, a corresponding ``vector'' parabolic equation can

Blanc-Benon, P. (2006) Outdoor Sound Propagation Modelling in Complex Environments: Recent Developments in the Parabolic Equation Method. In *Battlefield Acoustic Sensing for ISR Applications* (pp. 21-1 – 21-16). Meeting Proceedings RTO-MP-SET-107, Paper 21. Neuilly-sur-Seine, France: RTO. Available from: http://www.rto.nato.int/abstracts.asp.

Report Documentation Page

Form Approved
OMB No. 0704-0188

1. REPORT DATE	2. REPORT TYPE	3. DATES COVERED
01 OCT 2006	**N/A**	**-**

4. TITLE AND SUBTITLE	5a. CONTRACT NUMBER
Outdoor Sound Propagation Modelling in Complex Environments: Recent Developments in the Parabolic Equation Method	5b. GRANT NUMBER
	5c. PROGRAM ELEMENT NUMBER
6. AUTHOR(S)	5d. PROJECT NUMBER
	5e. TASK NUMBER
	5f. WORK UNIT NUMBER
7. PERFORMING ORGANIZATION NAME(S) AND ADDRESS(ES) **Ecole Centrale de Lyon Centre acoustique LMFA UMR CNRS 5509 36 Avenue Guy de Collongue 69134 ECULLY Cedex France**	8. PERFORMING ORGANIZATION REPORT NUMBER
9. SPONSORING/MONITORING AGENCY NAME(S) AND ADDRESS(ES)	10. SPONSOR/MONITOR'S ACRONYM(S)
	11. SPONSOR/MONITOR'S REPORT NUMBER(S)

12. DISTRIBUTION/AVAILABILITY STATEMENT
Approved for public release, distribution unlimited

13. SUPPLEMENTARY NOTES
See also ADM202421., The original document contains color images.

14. ABSTRACT

15. SUBJECT TERMS

16. SECURITY CLASSIFICATION OF:			17. LIMITATION OF ABSTRACT	18. NUMBER OF PAGES	19a. NAME OF RESPONSIBLE PERSON
a. REPORT	b. ABSTRACT	c. THIS PAGE			
unclassified	**unclassified**	**unclassified**	**UU**	**16**	

be derived for monochromatic sound waves. Recently Ostashev & al. ([2]), Dallois & al. ([3]), derived new wide-angle parabolic equations which do maintain the vector properties of the velocity of the medium. Significant progresses have been made in the modelling of sound propagation over distances ranging from hundreds meters to kilometers, and the agreement between calculated and measured fields have been greatly improved ([4], [5]).

In this paper we present a method which evaluates the propagation of an acoustic wave above an uneven terrain using a PE method and which includes realistic meteorological parameters. In our approach the effects of the topography are modelled using appropriate rotated co-ordinates systems in order to treat the ground as a succession of flat domains. We also examine the influence of scale resolution on numerical simulation of long range sound propagation through the turbulent atmosphere. Currently, we generate the turbulence using a Random Fourier Modes technique ([4], [6]), such that the turbulent fluctuation at any point in the medium (either scalar or vectorial in nature) is calculated from the sum of a chosen number of modes. Our model of outdoors sound propagation is validated both with classical numerical benchmark cases and recent experiments done in St-Berthevin where acoustical and meteorological measurements are performed simultaneously.

2.0 THEORETICAL BACKGROUND

During the last decade, propagation of sound above plane and heterogeneous grounds, including or not meteorological effects, has been extensively studied analytically, numerically and/or experimentally. Different numerical approaches such as Fast-Field Program without [7] and with turbulence [8], Boundary Element Methods [9,10, 11,12] and more recently, Meteo-BEM [13] have been successfully compared to analytical solutions and experiments for several usual situations. Nevertheless, when considering complex environments, mixed influence of terrain topography and atmospheric conditions has to be taken into account. In those particular situations where the propagation medium is not stationary with creation of mean motion or velocity fluctuations, numerical approaches based on parabolic equations seem to be well adapted to the problem. Different methods of resolution have been investigated. The main ones are: the Split-Step Fourier Method [14], the Crank-Nicholson scheme (CN-PE) [15, 16], the Green Function Parabolic Equation (GF-PE) [17, 18], the Generalized Terrain Parabolic Equation (GT-PE) [19], the Mean-Wind and Turbulent-Wind Wide-Angle Parabolic Equation (MW-WAPE, TW-WAPE) [2, 4].

In the recent years several authors have developed numerical simulations of sound propagation in the atmosphere taking into account atmospheric models. To model sound propagation in the atmospheric boundary layer the basic idea recently introduced is to use a mesocale atmospheric model to simulate local wind and temperature profiles in an area with complex topography of the terrain. This atmospheric model is couple with an appropriate model for sound propagation ([20, 21, 22]. Recently a different approach has been considered to improve the modelling of sound propagation in an inhomogeneous moving atmosphere ([23, 24]). These new numerical simulations are based on time–domain calculations performed with linearized equations of fluid dynamics. The interest of these finite-difference time-domain techniques are their ability to deal with complicated phenomena in outdoor sound propagation such as scattering by turbulence, 3D effects by buildings and topography ([41,42]). However a high computational effort is necessary to run these solvers and this approach is not yet appropriate to deal with long distance sound propagation problems. Among these techniques, a mixed method called "Split-Step Padé" has been validated [2, 25, 26]. It appeared to be reliable with respect to its obvious advantages in terms of angular aperture, CPU time and its capability to consider the main phenomena: from flat and homogeneous grounds to complex situations including mixed and/or uneven grounds.

2.1 Parabolic equation

The PE based methods seem to be the most appropriate to solve the problem of acoustic propagation above a mixed ground with topographical irregularities in a both refractive and turbulent

atmosphere. For numerical simulations of outdoor sound propagation, parabolic equations have been derived using the approximation of the effective sound speed to take into account the vectorial effect of the wind. In this conventional approach the real moving atmosphere is replaced by a hypothetical motionless medium with the effective sound speed $c_{eff}=c+v_x$, where v_x is the wind velocity component along the direction of sound propagation between source and receiver. This approach is convenient because both source and receiver are close to the ground and the preferred direction of sound is nearly horizontal. However, in many problems of atmospheric acoustics, refracted sound waves propagate in directions which may significantly differ from the direction of propagation ([5,27,28]). We use a specific PE developed by Ostashev *et al.* ([2]) and Dallois *et al.* ([3]) which does maintain the vector properties of the velocity medium.

We consider bi-dimensional (x, z) propagation of a monochromatic acoustic wave in a homogeneous and moving medium. If the length scale of the medium L is much greater than the acoustic length scale, $\lambda \ll L$, an exact wave equation for this situation in the frequency domain is given by Ostashev *et al.* ([2]):

$$\left[\Delta + k^2(1+\varepsilon) - \sqrt{1+\varepsilon}\,\frac{2ik}{c}\,\upsilon.\nabla + \frac{\upsilon_x \upsilon_z}{c^2}\,\frac{\partial^2}{\partial_x \partial_z}\right] p(r) = 0 \text{ , (Eq. 1)}$$

where: p is the acoustic pressure, $\omega=2\pi f$, f is the frequency, $k=\omega/c$, $\varepsilon=(c_0/c(r))^2-1$ is the variation of the standard refraction index, x and z are respectively the horizontal vertical directions, and $\boldsymbol{\upsilon}$ stands for the velocity of the medium. When $\boldsymbol{\upsilon}=0$, this equation is reduced to the Helmholtz equation:

$$\left[\Delta + k_0^{\,2}(1+\varepsilon)\right] p(r,\omega) = 0 \text{ . , (Eq. 2)}$$

The additional terms in Eq. (1) compared to Eq. (2) contain the effects of the moving medium. Ostashev *et al.* ([2]) and Dallois *et al.* ([3]) reduced Eq. (1) to wide-angle parabolic equation. The first step is to write the 2D equation for forward propagation ([2,3]):

$$\left[\frac{\partial}{\partial x} - ik\sqrt{Q}\right] p(r,\omega) = 0. \text{ , (Eq. 3)}$$

From here, the pseudo-operator $\sqrt{Q}$ is simplified using a Padé approximation to yield:

$$\sqrt{Q} = \frac{1+pL}{1+qL}, \quad \text{(Eq. 4)}$$

where L=Q-1, p=3/4 and q=1/4. Considering the envelope of the pressure field defined as $\phi(r)=p(r)\exp(-ikx)$, the parabolic equation turn to mean-wind wide-angle parabolic equation (MW-WAPE):

$$\begin{aligned}&\left[1 + qF_1 - ipkM_1 - qk^2 M_1^2\right]\frac{\partial \phi}{\partial x} \\ &= ik\left[(p-q)F_1 + ik(p-q)M_1 - ikM_1F_1 + qk^2M_1^2\right]\phi,\end{aligned} \quad \text{(Eq.5)}$$

where:

$$F_1 = \frac{1}{c^2 - v_x^2}\left[c_0^2 + 2ic_0\frac{v_z}{k}\frac{\partial}{\partial z} + \frac{c^2 - v_z^2}{k^2}\frac{\partial^2}{\partial z^2}\right] - 1,$$

$$M_1 = \frac{2v_x}{k(c^2 - v_x^2)}\left[ic_0 - \frac{v_z}{k}\frac{\partial}{\partial z}\right].$$

If all velocities in Eq. (5) are set to zero, this equation is reduced to the classical Padé (1, 1) PE (WAPE) derived from Helmholtz equation (2):

$$[1 + qL]\frac{\partial\phi(r)}{\partial x} = ik_0[(p - q)L]\phi(r), \quad \text{(Eq.6)}$$

where:

$$L = \varepsilon_{eff} + \frac{1}{k}\frac{\partial^2}{\partial z^2}, \quad \text{(Eq. 7)}$$

with

$$\varepsilon_{eff} = n_{eff}^2 - 1 = c_0^2 / c_{eff}^2 - 1. \text{ (Eq. 8)}$$

Eq. (3) and Eq. (5) are discretized on a uniform mesh (iΔx, jΔz) using a standard finite difference method. z-derivatives are evaluated by centered difference approximations, and Crank-Nicholson scheme is implemented as a marching algorithm which takes the following form:

$$A\phi(x + \Delta x, z) = B\phi(x, z), \text{ (Eq. 9)}$$

where A and B are pentadiagonal (MW-WAPE) or triagonal (WAPE) matrices. In our computations, the ground is modeled as a locally reacting surface with finite complex impedances calculated using the one parameter approximation from Delany and Bazley ([29]). Reflexions at the top of the numerical grid are controlled by introducing a thin artificial absorption layer in the upper part of the computation domain. The uneven terrain is treated as a succession of flat domains ([26, 30, 31]). After each flat domain the coordinate system (x,z) is rotated so that the x axis remains parallel to the ground (figure 1) .The calculation above each domain needs an initial solution. The values of the initial solution for the domain n+1 are obtained from the interpolated values of the pressure field of the domain n, except for the first domain where the source is initialized by a Gaussian starter which has an adjustable width and takes into account the image source weighed by a complex reflection coefficient.

In order to validate the method, we consider the propagation above a wedge. A reference solution can be established analytically as the sum of a geometrical field and a diffracted field ([26]). We consider the case of a positive slope and of a negative slope. We chose d1=60 metres, d2=40 meters and alpha=20 degrees. The unit point source is located at 2 meters above the ground. The acoustic frequency is 340 Hz. On figures 2 and 3 we compare two analytical solutions and the PE solution. We evaluate the pressure amplitude on the same benchmark case on a line L perpendicular to the slope at 40 meters of the bottom discontinuity.

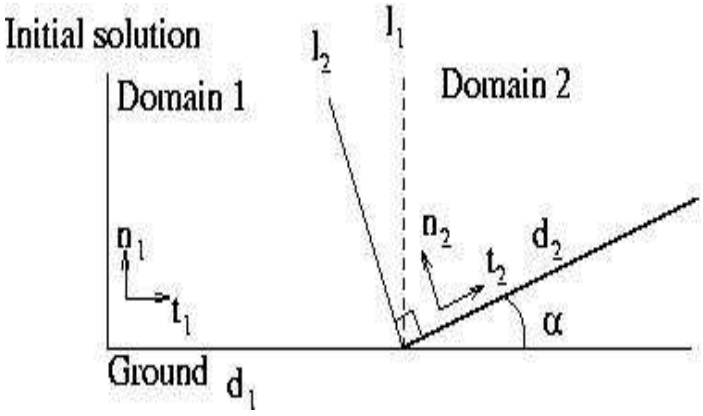

Figure 1 - Definition of the computational domains.

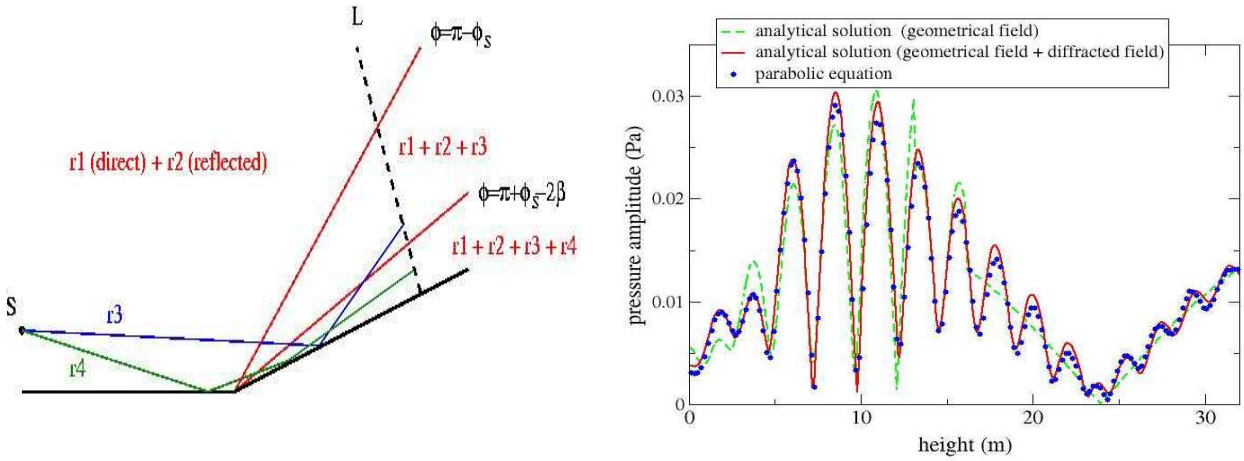

Figure 2: Sound propagation for an upslope wedge (hs=2 m.;d1=60 m. , d2=40m.).

The first analytical solution is the geometrical part of the pressure; the second is the total analytical pressure field (geometrical plus diffracted). The agreement between the PE solution and the first analytical solution (geometrical plus diffracted field) is excellent in both cases (upslope and downslope). The difference between the two analytical solutions is due to diffracted part of the pressure field. We conclude that the rotated PE method calculates accurately the diffracted part of the field above the wedge. Others numerical comparisons in the cases of the curved surfaces have been done ([26,30]) : the rotated PE method gives accurate results until a angle of 40 degrees and for frequencies between 100 and 3200 Hz.

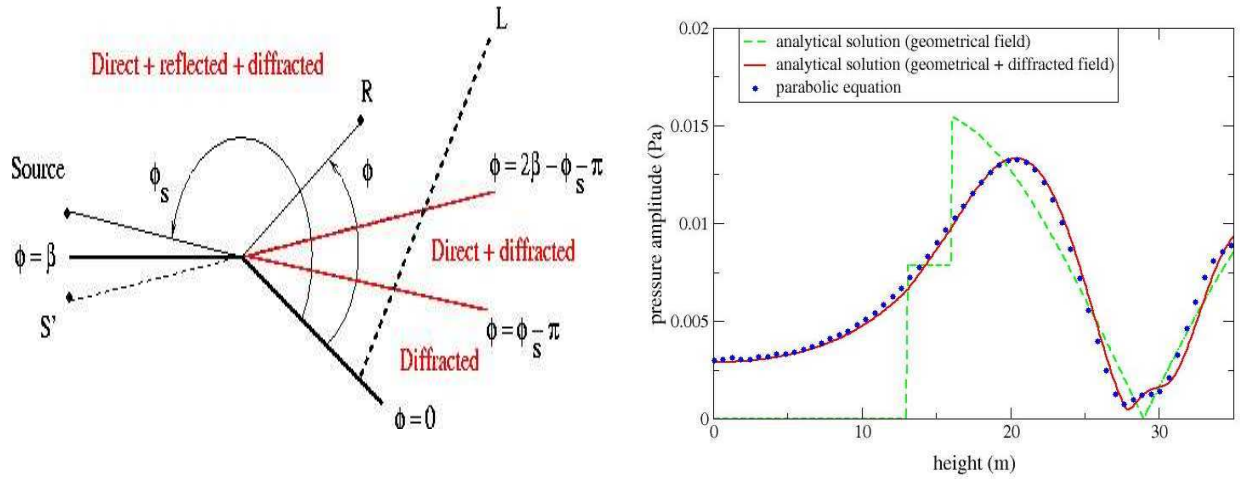

Figure 3: Sound propagation for a downslope wedge (hs=2 m. ,d1=60 m., d2=40 m..)

2.2. Atmospheric model

There are several ways of modelling the vertical wind and temperature profiles near the ground: linear, logarithmic, multi-linear, linear-logarithmic, hybrid, etc. As first order approximations, temperature and wind profiles are set constant with distance (non range dependent) on each flat domain. Likewise the profiles are slightly rotated with each corresponding domain, since the angles between the rotated systems of coordinates are very small (inferior to 5°). Moreover, following Panofsky & Dutton ([32]) and Gilbert & White ([15]), temperature and wind profiles are assumed to be logarithmically shaped and expressed as:

$$T(z) = T(z_0 + d) + a_T \ln(\frac{z-d}{z_0}),$$
$$v(z) = a_v \ln(\frac{z-d}{z_0}), \quad \text{(Eq. 10)}$$

where d is the displacement length, z_0 is the roughness parameter, a_T and a_v are refraction parameters related to temperature and wind respectively. The effective sound speed c_{eff} used in the classical Padé (1,1) PE [Eq. (8)] is defined from wind and temperature fields as:

$$c_{eff}(z) = c_0\sqrt{1+\frac{T(z)}{273.15}} + v(z)\cos(\theta), \text{ (Eq. 11)},$$

$$c_{eff}(z) \approx c_0(1+\frac{1}{2}\frac{T_0}{273.15}) + \left(\frac{1}{2}\frac{c_0}{273.15}a_T + \cos(\theta)a_v\right)\ln(\frac{z-d}{z_0}), \text{ (Eq. 12)}$$

where c_0 is the sound speed for T=273.15K (≈331m/s) and θ is the angle between wind direction and the direction of sound propagation. We can define an effective refraction parameter a_{eff} as follow:

$$a_{eff} = \frac{1}{2}\frac{c_0}{273.15}a_T + cos(\theta)a_v . \quad \text{(Eq. 13)}$$

This effective refraction parameter is used with WAPE while temperature and wind refraction parameters are used with MW-WAPE. Our MW-WAPE code needs accurate propagation conditions as input data for calculations. Vertical sound speed profiles could be determined from wind and temperature profiles through data post-processing of experimental data. Those profiles can be also numerically synthesized by a micrometeorological model. This has been carried out in the context of road traffic noise using an atmospheric code called SUBMESO ([22]). MW-WAPE can also deal with turbulence; we generate the turbulence using a Random Fourier Modes technique, such that the turbulent fluctuation at any point in the medium (either scalar or vectorial in nature) is calculated from the sum of a chosen number of modes with an amplitude distributed according to a prescribed energy spectrum ([4, 6, 33]).

2.3 Sound scattering in an upward-refracting turbulent atmosphere

In an upward-refracting atmosphere, acoustic energy is scattered into the shadow zone due to temperature and wind fluctuations. The strength of this scattering not only depends on turbulence parameters (i.e. turbulence scales and variance of refractive-index fluctuations) but also on the acoustic frequency and geometry (range, source and receiver heights) considered. As shown in previous studies ([33,34,35,37]), there is a coupling between turbulence parameters, acoustic frequency and geometry, which means that the turbulence scales involved in the scattering of acoustic energy into the shadow zone also depend on acoustic frequency and geometry. The smallest turbulent structures involved in acoustic scattering into the shadow zone can be found using Bragg's relation, which links angle of diffraction of acoustic energy with acoustic frequency and turbulent structure/eddy size. The range of acoustic frequencies of interest is thus relatively large (from 50Hz to 4kHz), and the range relatively long (up to 1km). To predict sound pressure levels given these constraints, numerical simulations are realized using a wide-angle PE code including turbulence effects [4, 31, 33]. Turbulence is generated using a Random Fourier Mode (RFM) technique assuming frozen turbulent fluctuations. Mode orientations and phases are independent random variables chosen to yield homogeneous isotropic fields. For each realization, temperature (or velocity) fluctuations are obtained by summing over a limited number of random Fourier modes. In the simulations the sound pressure level is averaged over 30 realizations, which is enough to obtain accurate results [4]. In this paper the simulations are done in a two-dimensional space, and only temperature fluctuations are considered. Temperature is decomposed into a mean part $\overline{T} = T_0$ and a fluctuating part T': $T = T_0 + T'$. The turbulent thermal energy spectrum G is modelled by a modified von Kármán spectrum of the form [4, 33, 40]:

$$G^{3D}(K) = 4\pi A {C_T}^2 K^2 \left[K^2 + \frac{1}{{L_0}^2}\right]^{-11/6} \exp\left(-\frac{K^2}{K_m^2}\right), \quad \text{(14a)}$$

$$G^{2D}(K) = \frac{5}{3}\frac{\overline{T'^2}}{L_0^{5/3}} K \left[K^2 + \frac{1}{{L_0}^2}\right]^{-11/6} \exp\left(-\frac{K^2}{K_m^2}\right), \quad \text{(14b)}$$

in three- and two-dimensions, respectively, with K the turbulent wave number, $K_m = 5.92/l_0$, L_0 and l_0 the outer and inner scales of turbulence, respectively, $A \approx 0.0330$, and ${C_T}^2 \approx 1.91\overline{T'^2}/L_0^{2/3}$. Expressions can also be written in terms of the index of refraction n, $n = \overline{n} + \mu$, where μ is the fluctuating part. For small fluctuations μ is written as: $\mu \approx T'/2T_0$. In the PE code, the spectrum given by Equation (14b) is used for consistency with two-dimensional geometry. Turbulence parameters for all simulations are: $L_0 = 5m$, $l_0 = 0.05m$, and $\overline{\mu^2} \approx 10^{-5}$ (corresponding to a temperature standard

deviation of 1.8K).

2.3.1. Scattering cross-section

The scattering cross-section characterizes the amount of acoustic power scattered by a volume of inhomogeneities (or scattering volume) per unit incident acoustic intensity and per unit volume: $\sigma^{3D} = r^2 \overline{I_S} / I_0 V$, with the notations of Figure 1, $\overline{I_S}$ the mean scattered acoustic intensity, and I_0 the incident acoustic intensity. The scattering cross-section characterizes the angular dependence of acoustic scattering by turbulence; it has the dimension of m^{-1}. When considering temperature and velocity fluctuations, the scattering cross-section for homogeneous turbulence is written [36]:

$$\sigma^{3D} = 2\pi k^4 \cos^2\theta \left(\frac{1}{4T_0^2} \Phi_T^{3D}\left(k(\vec{m}_0 - \vec{m})\right) + \frac{m_{0i} m_{0j}}{c_0^2} \Phi_{ij}^{3D}\left(k(\vec{m}_0 - \vec{m})\right) \right) , \tag{15}$$

where k is the acoustic wave number, T_0 and c_0 are the mean temperature and sound speed, respectively, and Φ_T^{3D} and Φ_{ij}^{3D} are the three-dimensional spectral densities of the fluctuations of temperature and of the i^{th} and j^{th} components of velocity, respectively. This expression is obtained assuming that the propagation distances r_0 and r are large with respect to the scale of the inhomogeneities L, and L is large with respect to the acoustic wavelength λ. Writing σ_T the scattering cross-section only due to temperature fluctuations, it comes for homogeneous and isotropic turbulence in three- and two-dimensions:

$$\sigma_T^{3D}(\theta) = \frac{k^2}{32T_0^2} \frac{\cos^2\theta}{\sin^2\theta/2} G^{3D}\left(2k\left|\sin\theta/2\right|\right) , \tag{16a}$$

$$\sigma_T^{2D}(\theta) = \frac{k^2}{8T_0^2} \frac{\cos^2\theta}{\left|\sin\theta/2\right|} G^{2D}\left(2k\left|\sin\theta/2\right|\right) . \tag{16b}$$

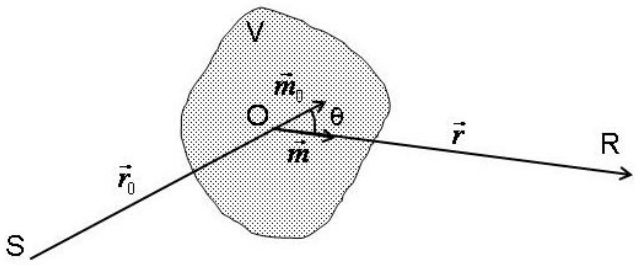

Figure 4: Geometry of source S, receiver R, scattering volume V and scattering angle θ.

Equations (16a) and (16b) show that scattering at the angle θ only depends on spectral components of the turbulence with wave numbers $2\pi/L = 2k\sin\theta/2$. This can be rewritten:

$$\lambda = 2L\sin\theta/2 , \tag{17}$$

which satisfies Bragg's condition . Bragg's relation given in Equation (17) is useful since it estimates the main turbulent structure size L responsible for the scattering at the angle θ for a given acoustic wavelength

λ. Several authors already used this relation to interpret numerical results of acoustic scattering by turbulence [33, 34, 35, 37]. In Figure 5 we compare the scattering cross-sections in 2D and 3D calculated at two different acoustic frequencies. The scattering cross-sections are seen to reach their maximum at θ equal to zero (forward-scattering). For the higher acoustic frequency of 1600Hz, small scattering angles (below 5 to 10 degrees) contain most of the scattered energy. This is less pronounced at the lower acoustic frequency of 100Hz. It also appears that 2D expressions are lower than 3D ones, although there is a simple relation of proportionality between the two. As a result the normalized scattering cross-sections are the same in the two- and three-dimensional case.

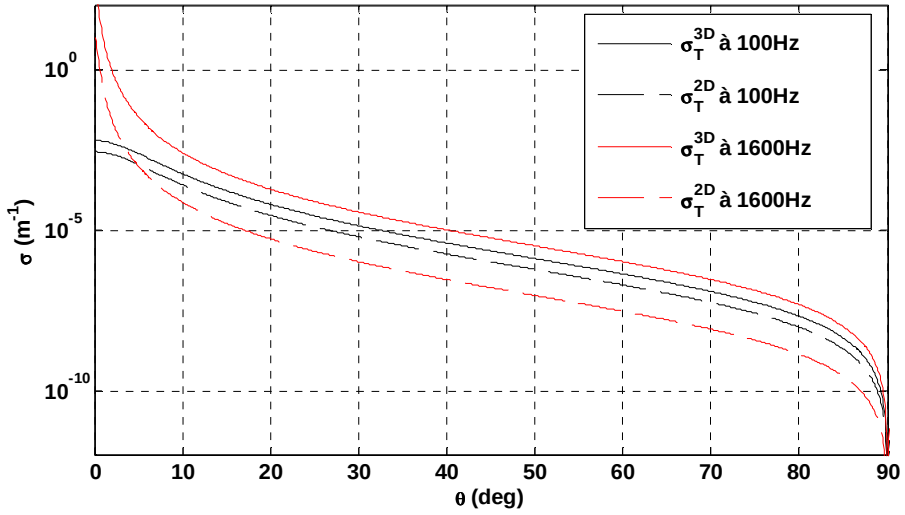

Figure 5: Scattering cross-sections at 100Hz (black) and 1600Hz (red) in three- (solid lines) and two- (dashed lines) dimensional space. Temperature fluctuations are modeled with the modified von Kármán spectrum .

2.3.2. Influence of cut-off turbulent wave numbers on sound propagation

Let $\Delta L = 10\log_{10}\left(p^2 / p_{free}^2\right)$ be the relative sound pressure level, where p is the acoustic pressure calculated, and p_{free} is the acoustic pressure in free space and in homogeneous propagation conditions. In order to obtain the third octave band spectrum of the sound pressure level between 50Hz and 1600Hz, 46 frequencies are calculated to have a 1dB maximum error. All simulations are run with a source height of 2m, a porous ground with an effective flow resistivity of 200kN.s.m^{-4}, typical of grassland, and a logarithmic sound speed profile $c(z) = c_0 + a_{\log}\ln(1 + z/z_0)$, with $c_0 = 340m/s$, $a_{\log} = -2.1m/s$, and $z_0 = 0.1m$. This sound speed profile is representative of a strong sound speed gradient. We focus on the influence of the small turbulent structures. Part of the approach presented here follows Wert *et al.* [33]. From the scattering cross-sections plotted in Figure 5, we expect that only small scattering angles have a significant effect on scattering into the shadow zone. Using Bragg's relation of Equation 17, smaller and smaller structures are likely to be involved when the acoustic frequency increases. This qualitative reasoning is confirmed by numerical simulations. In the PE simulations, different maximum turbulent wave numbers $K_{C\max}$, from 1m^{-1} to 32m^{-1}, are considered. Figure 6 shows the difference in the 800Hz third octave band relative sound pressure level between simulations with $K_{C\max}$ equal to 32m^{-1} (taken as the reference simulation) and 2m^{-1}. Clearly in the latter case the sound pressure level in the shadow zone is smaller, which shows that turbulent wave numbers between 2 and 32m^{-1} are important.

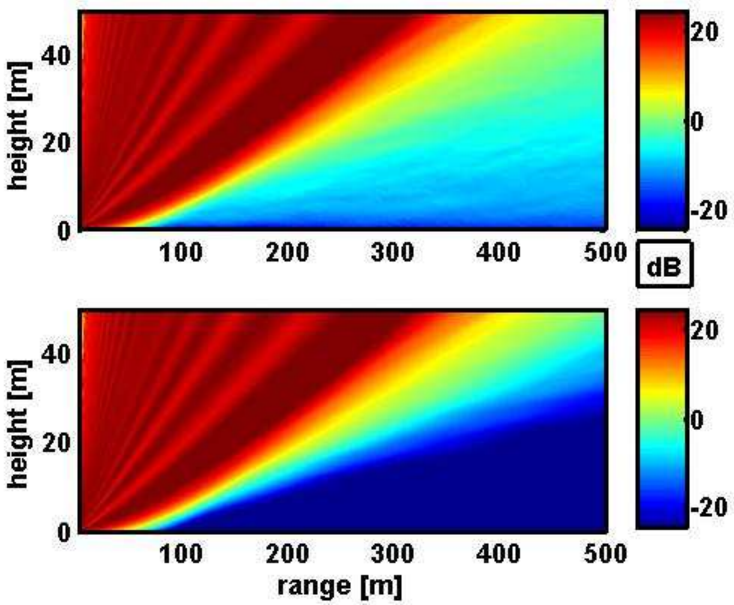

Figure 6: Relative sound pressure level ΔL for $K_{C\max} = 32m^{-1}$ (top) and $K_{C\max} = 2m^{-1}$ (bottom) on the 800Hz third octave band.

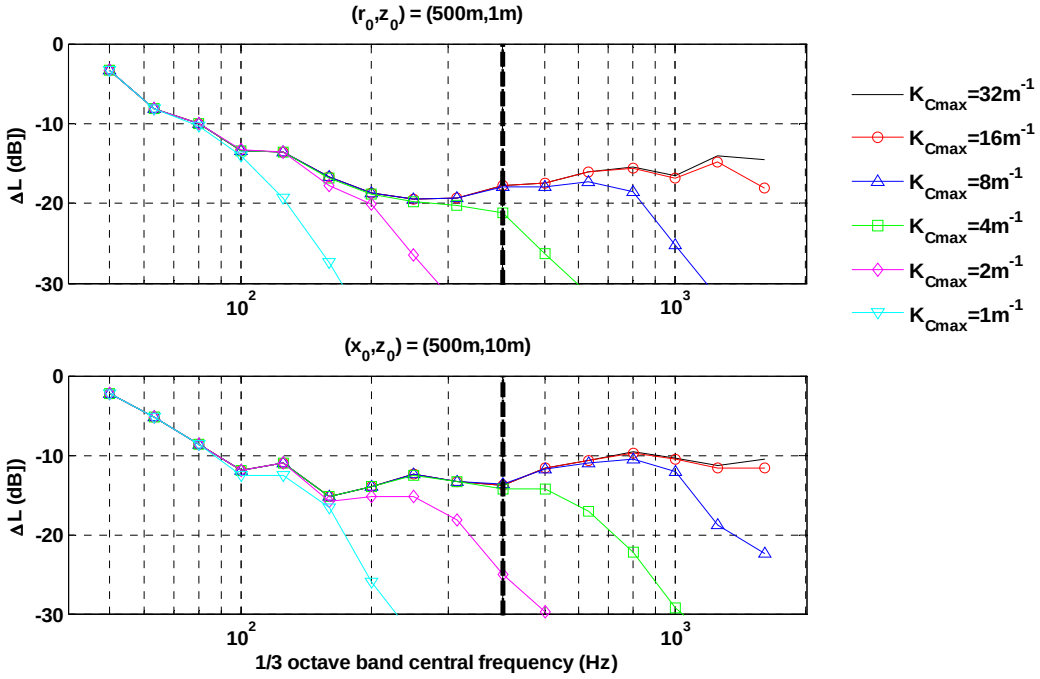

Figure 7: Third octave band spectrum of the relative sound pressure level ΔL at a receiver located at (r0,z0) (as given on top of each plot) with $K_{C\max}$ as given. A black vertical line is plotted at 400Hz.

To be more specific, we compare the third octave band spectra of the relative sound pressure level from the simulations with different $K_{C\max}$ at a range of 500m and at two heights in Figure 7. Below 100Hz approximately, the receiver is still located in the illuminated region and all simulations give the same

results. When acoustic frequency increases above 100Hz, $K_{C\max}$ needs to be increased to reach the reference simulation. For instance in the 400Hz band (see the black vertical lines in Figure 7), only simulations with $K_{C\max} \geq 8m^{-1}$ are acceptable at a height of 1m. At a height of 10m, the simulation with $K_{C\max}$ equal to $4m^{-1}$ is also acceptable. At greater heights the receiver is not as deep in the shadow zone, thus sound pressure levels are higher and the condition on the maximum turbulent wave number is not as critical as at a lower height. These results show that the maximum cut-off turbulent wave number increases with acoustic frequency. From the 1m height plot we see that simulations with $K_{C\max}$ equal to $1m^{-1}$, $2m^{-1}$, $4m^{-1}$, $8m^{-1}$, $16m^{-1}$ are roughly valid up to the 63Hz, 125Hz, 250Hz, 500Hz and 1kHz third octave bands, respectively, where validity is understood here as closeness to the reference simulation. Thus there appears to be a more or less linear dependence between the two quantities: $K_{C\max} \propto f$. This is consistent with Bragg's relation considering a maximum scattering angle that is constant with respect to acoustic frequency.

3.0 SOUND PROPAGATION IN A COMPLEX REALISTIC ENVIRONMENT

An outdoor site near Saint Berthevin (France) has been selected to study the influence of meteorological conditions on sound propagation. This offers the possibility of simultaneous detailed measurement of meteorological and noise propagation data as indicated on figure 8. The meteorological data are collected on towers M1 to M7 and the sound pressure levels are measured on towers A1 to A5. Meteorological data and sound levels at the receivers are recorded simultaneously. (Additional details are available in [22, 26]). This survey provides a database of noise level variations in a complex environment (non flat terrain, mixed ground) and thus allow us to validate our numerical simulation of outdoors sound propagation.

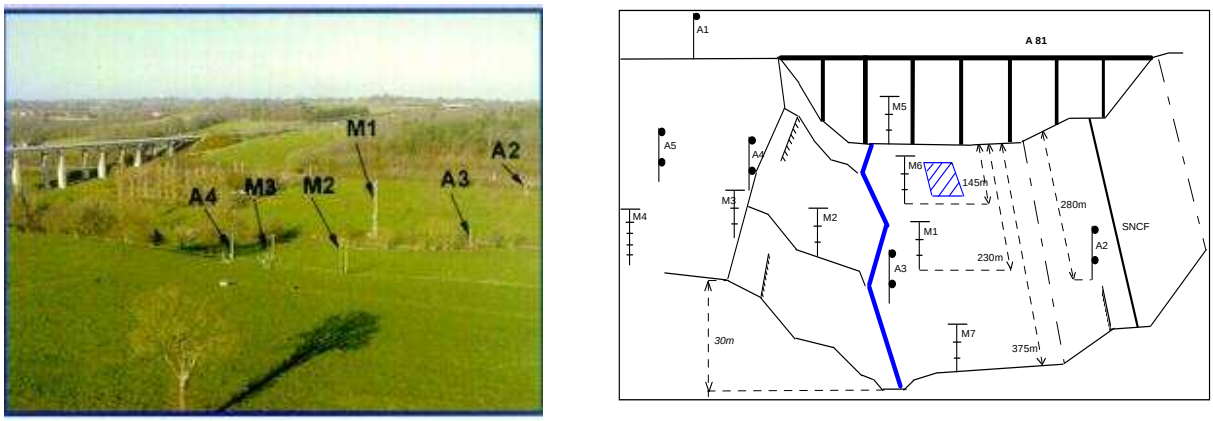

Figure 8 View of St Berthevin and schematic illustration of the experimental set-up

The terrain is modelled using a succession of six flat domains with finite complex impedance Z. Z is calculated using the one-parameter formula of Delany-Bazley ([29]):

$$Z = \rho_0 c_0 \left(1 + 0.0571 \left(\frac{\rho_0 f}{\sigma} \right)^{-0.754} + i 0.087 \left(\frac{\rho_0 f}{\sigma} \right)^{-0.732} \right), \text{(Eq. 18)}$$

where f is the frequency and σ is the flow resistivity. A broadband source is located at 2m from the ground, the reference level is calculated in front of the source at a distance of 1m (see figure 9). In order to evaluate the micrometeorological conditions, we used an equipped tower located on the slope but far enough from the measurement line not to disturb acoustic propagation. The tower is equipped with ventilated air thermometers (YOUNG 41342VC) and accurate wind direction and wind speed sensors (YOUNG 05305AQ), using a YOUNG 26700 station. The accuracy is about 0.1°C, 2° and 0.1m/s respectively. The sampling rates of the temperature and wind measurements are too low as to derive turbulence parameters. These sensors are located at 3 different heights: 1, 3 and 10m. Temperature and wind profiles are modelled following Eq. (10), where a_T and a_v are deduced from micrometeorological measurements (10min average). For each acoustical measurement, the signal has been averaged over 10 gun shots, which is a sufficient number to determine a reliable average value for acoustical measurements. Results are given in terms of relative Sound Pressure Level coming from the difference between the spectrum at microphone M1, M2, M3, M4 or M5 and the spectrum at the reference microphone M_{ref}.

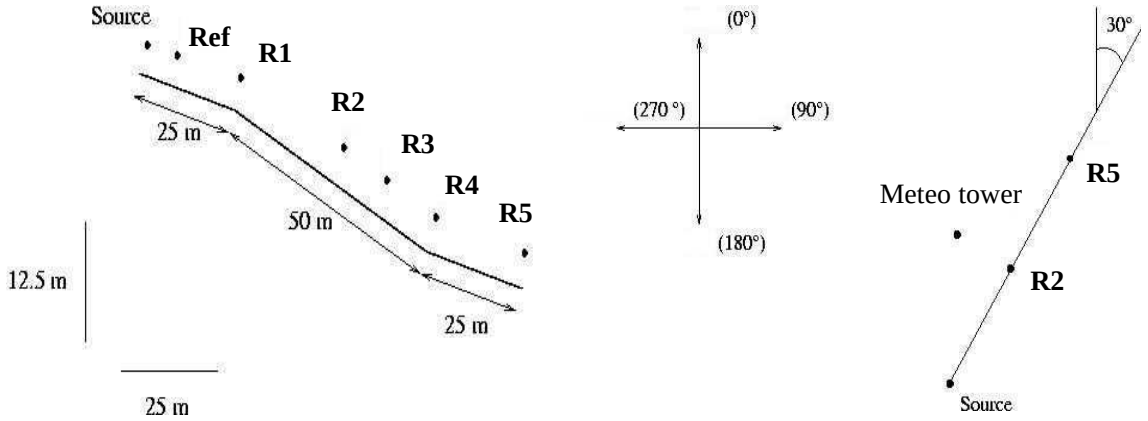

Figure 9 Experimental set-up .The source and the receivers R1 – R5 are located 2 m above the ground, the angle between the wind direction and the axis of propagation is 20°.

Figure 10 gives a comparison between experimental data measures at St Berthevin and numerical simulations calculated with PE. In the results presented here, the micrometeorological parameters deduced from experimental data are : the angle between wind direction and the direction of sound propagation θ =20°, the refraction parameters related to temperature and wind respectively a_T=0.20 and a_v=0.65 , and the effective refraction parameter a_{eff}=0.73. The characteristic impedance value of each domain of the ground surface has been determined according to the grazing incidence technique developed by Bérengier and Garai ([38]). This measurement technique requires a set of two microphones located 4 m away from an impulse source. The estimation of the airflow resistivity value of the ground to be qualified is obtained through a Levenberg-Marquardt inverse fitting algorithm applied to the experimental narrow-band excess attenuation between the two microphones ([39]). The results of the fitting procedures for downslope propagation are : σ = 600 Pa·s·m^{-2} around the source, σ = 90 Pa·s·m^{-2} around M1, σ = 160 Pa·s·m^{-2} around M2 and σ = 200 Pa·s·m^{-2} around M4. The distances of propagation are respectively 25 m for the receiver

R2 and 75m for the receiver R5. At the receiver R5 placed down the hill we clearly observed the influence of the wind (see figure10). If the mean wind profile is not taken into account in the numerical simulation we noted large differences between the measured data and the estimated sound pressure level; at large distance of propagation (R5) and for high frequencies (above 500 Hz) the difference is of the order of 15dB. When the mean velocity profile is taken into account in the PE simulation, the agreement between calculated and measured values is reasonable. The differences could be attributed to the variations of the local impedance, and to the fluctuations of the meteorological parameters (mainly the wind direction and the turbulence). Concerning the back-scattered sound energy by slopes, Blairon ([26]) showed that the ratio between the scattered and the total acoustic energy is less than 0.1 % for a frequency of 500 Hz and a slope of 40 degrees.

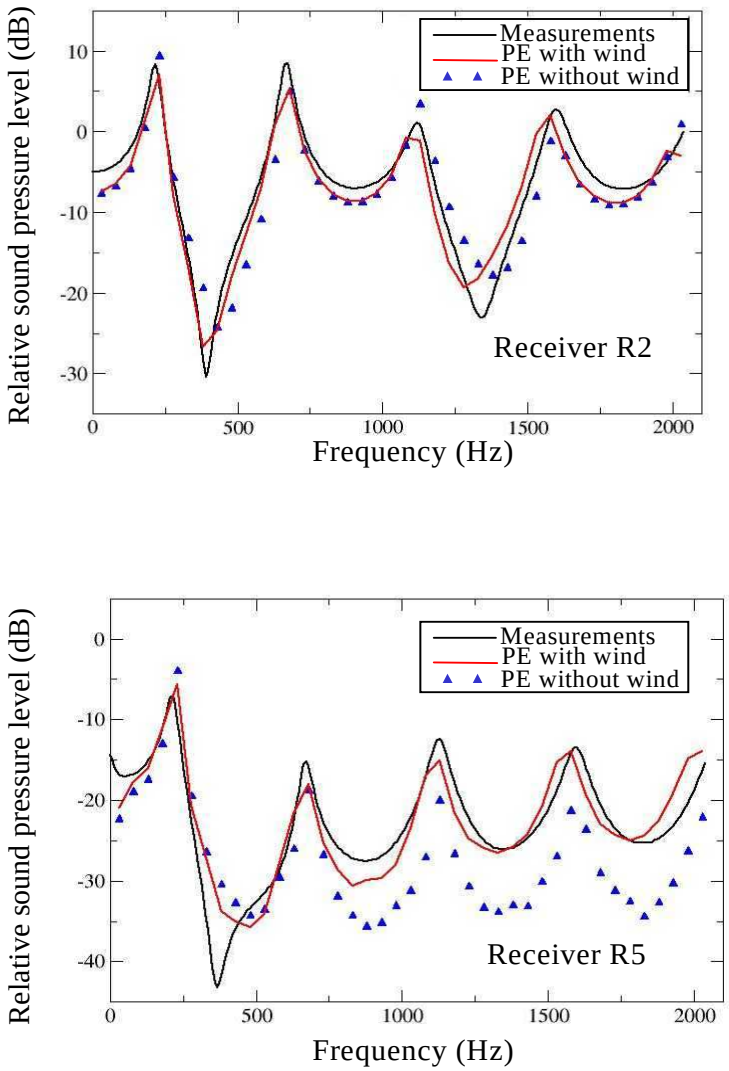

Figure 10 Relative sound pressure levels measured at two receivers R2 and R5. Comparisons with numerical estimated calculated using the PE method: influence of the mean wind.

4.0 CONCLUSION

In this paper we have presented a method which evaluates the propagation of an acoustic wave above an uneven terrain using wide-angle parabolic equations which do maintain the vector properties of the velocity of the medium and which includes realistic meteorological parameters. In our approach the effects of the topography are modelled using appropriate rotated co-ordinates systems in order to treat the ground as a succession of flat domains. We also examine the influence of scale resolution on numerical simulation of long range sound propagation through the turbulent atmosphere. Currently, we generate the turbulence using a Random Fourier Modes technique ([4], [6]), such that the turbulent fluctuation at any point in the medium (either scalar or vectorial in nature) is calculated from the sum of a chosen number of modes. An outdoor site near Saint-Berthevin (France) has been selected to study the influence of meteorological conditions on noise traffic. Acoustical and meteorological measurements are performed simultaneously. This survey provides a database of noise level variations in a complex environment (non-flat terrain, mixed ground). The agreement we obtained between our numerical simulation based on a PE model and the measured data can be considered as very promising. Work is currently in progress to study over long time periods the statistical effects of meteorology on long range sound propagation.

5.0 ACKNOWLEDGEMENT

This research is partially supported by Laboratoire Central des Ponts et Chausées.

6.0 REFERENCES

[1] T. F. W. Embleton, " Tutorial on sound propagation outdoors", J. Acoust. Soc. Am 100(1), 31-48, (1996).

[2] V.E. Ostashev, D. Juvé , Ph. Blanc-Benon , "Derivation of a wide-angle parabolic equation for sound waves in inhomogeneous moving media", Acustica united with Acta Acustica, Vol 83(3), pp 455-460,1997.

[3] L. Dallois, Ph. Blanc-Benon , D. Juvé, "A wide angle parabolic equation for sound waves in inhomogeneous moving media: applications to atmospheric sound propagation", J. Comp. Acous., Vol. 9(2), pp 477-494, 2001.

[4] P. Chevret, Ph. Blanc-Benon , D. Juvé, "A numerical model for sound propagation through a turbulent atmosphere near the ground ", J. Acous. Soc. Am. , Vol. 100, pp 3587-3599, 1996.

[5] Ph. Blanc-Benon, L. Dallois, D. Juvé, "Long range sound propagation in a turbulent atmosphere within the parabolic approximation", Acustica united with Acta Acustica, Vol 87(1), pp 659-669, 2001

[6] M. Karweit, Ph. Blanc-Benon, D.Juvé , G. Comte-Bellot , "Simulation of the propagation of an acoustic wave through a turbulent velocity field: A study of phase variance", J. Acoust. Soc. Am 89(1), 52-62, (1991).

[7] R. Raspet, S.W. Lee, E. Kuester, D.C Chang, W.F. Richards, R. Gilbert, N. Bong , "A fast-field program for sound propagation in a layered atmosphere above an impedance ground". J. Acoust. Soc. Am. 77 (1985) 345-352.

[8] R. Raspet, W. Wu, "Calculation of average turbulence effects on sound propagation based on the fast-field program formulation". J. Acoust. Soc. Am. 97 (1995) 147-153.

[9] S.N. Chandler-Wilde, D.C. Hothersall, "Sound propagation above an inhomogeneous impedance plane". J. Sound and Vib. 98 (1985) 475-491.

[10] S.N. Chandler-Wilde, D.C. Hothersall, "Efficient calculation of the Green function for

acoustic propagation above a homogeneous impedance plane". J. Sound and Vib. 180 (1995) 705-724.

[11] F. Anfosso-Lédée, P. Dangla, "Modélisation numérique du fonctionnement des écrans antibruit routiers dans leur environnement". Bulletin des Laboratoires des Ponts et Chaussées. 203 (1996) 45-54.

[12] P. Boulanger, T. Waters-Fuller, K. Attenborough, K.M. Li, "Models and measurements of sound propagation from a point source over mixed impedance ground". J. Acoust. Soc. Am. 102 (1997) 1432-1442.

[13] E. Premat, Y. Gabillet, "A new boundary-element method for predicting outdoor sound propagation and application to the case of sound barrier in the presence of downward refraction". J. Acoust. Soc. Am. 108 (2000) 2775-2783.

[14] F.D. Tappert, R.H. Hardin, "Computer simulation of long range oceanic acoustic propagation using the parabolic equation method". 8th Int. Congress on Acoustics, London, UK. (1974) 452.

[15] K.E. Gilbert, M.J. White, "Application of the Parabolic Equation to sound propagation in a refracting atmosphere". J. Acoust. Soc. Am. 85 (1989) 630-637.

[16] J.M. Craddock, M.J. White, "Sound propagation over a surface with varying impedance: A Parabolic Equation approach". J. Acoust. Soc. Am. 91 (1992) 3184-3191.

[17] X. Di, K.E. Gilbert, "Application of a Fast Green's function method to long range sound propagation in the atmosphere". 5th Int. Symp. on Long Range Sound Propagation, Milton Keynes, UK, (1992) 128-141.

[18] E.M. Salomons, "Improved Green's function parabolic equation method for atmospheric sound propagation". J. Acoust. Soc. Am. 104 (1998) 100-111.

[19] R.A. Sack, M. West, "A parabolic equation for sound propagation in two dimensions over any smooth terrain profile: the generalized terrain parabolic equation (gt-pe)". Applied Acoustics 45 (1995) 113-129.

[20] L.R. Hole , G. Hauge , "Simulation of a morning air temperature inversion break-up in complex terrain and the influence on sound propagation on a local scale", Applied Acoustics, 64, 401 - 414, (2003).

[21] D. Heimann, G. Gross , "Coupled simulation of meteorological parameters and sound level in a narrow valley", Applied Acoustics, 56, 73 - 100, (1999).

[22] B.Lihoreau, B. Gauvreau , Ph. Blanc-Benon, I. Calmet., M. Bérengier, " Outdoor sound propagation modeling in realistic environments: a coupling method using MW-WAPE and SUBMESO",J. Acoust. Soc. Amer., 120 (1), 110-119, (2006).

[23] R. Blumrich , D. Heimann D., "A linearized Eulerian sound propagation model for studies of complex meteorological effects", J. Acoust. Soc. Am 112, 446-455, (2002).

[24] V.E. Ostashev, D.K. Wilson, L. Liu, D.F. Aldridge, N.P. Symons, D. Martin, "Equations for finite-difference, time-domain simulation of sound propagation in moving inhomogeneous media and numerical implementations", J. Acoust. Soc. Am 117, 503-517, (2005).

[25] M.D. Collins, "A split-step Padé solution for the parabolic equation method", J. Acoust. Soc. Am. , 93 ,(1993) 1736-1742.

[26] N. Blairon,"Topography effect on acoustic propagation in the atmosphere: Numerical modelization using parabolic equation and validation by comparison with outdoor experiments," (in French) Ph.D. thesis, École Centrale de Lyon, 2002-57, France (2002).

[27] O.A. Godin, "Wide-angle parabolic equation for sound in 3D inhomogeneous moving medium," Dokl. Phys. 47, 643–646 (2002).

[28] J.F. Lingevitch, M.D. Collins, D.K. Dacol, D.P. Drob, "A wide angle and high Mach number parabolic equation," J. Acoust. Soc. Am. 111, 729–734 (2002)
[29] M.E.Delany and E.N Bazley, “Acoustical properties of fibrous absorbent materials”, Appl. Acoust. 3, 105-116, (1970).
[30] N. Blairon, Ph. Blanc-Benon, M. Bérengier, D. Juvé, "Outdoor sound propagation in complex environment: experimental validation of a PE approach," Proceedings of the 10th Int. Symp. on Long Range Sound Propagation, Grenoble, France, 114–128 (2002).
[31] B. Gauvreau, M. Bérengier, Ph. Blanc-Benon, C. Depollier, "Traffic noise prediction with the parabolic method: Validation, of a split-step Padé approach in complex environments," J. Acoust. Soc. Am. 112, 2680–2687 (2002).
[32] H.A. Panofsk, J.A. Dutton, *Atmospheric Turbulence*, Ed. Wiley, New York, 1984.
[33] K. Wert, Ph. Blanc-Benon and D. Juvé, “Effect of turbulence scale resolution on numerical simulation of atmospheric sound propagation,” AIAA/CEAS Paper N° 98-2245, 4th AIAA/CEAS Aeroacoustics Conference, Toulouse, 1998.
[34] M.R. Stinson, D.I. Havelock and G.A. Daigle, “Simulation of scattering by turbulence in to a shadow region using the GF-PE method,” 6th LRSP, Ottawa NRCC, 283-295, 1994.
[35] D.K. Wilson, J.G. Brasseur and K.E. Gilbert, “Acoustic scattering and the spectrum of atmospheric turbulence,” Journal of the Acoustical Society of America, 105, 30-34 (1999).
[36] V. Ostashev, “Sound propagation and scattering in media with random inhomogeneities of sound speed, density and medium velocity,” Waves in Random Media, **4**, 403-428 (1994).
[37] D. Juvé, Ph. Blanc-Benon, P. Chevret , "Numerical simulation of sound propagation through a turbulent atmosphere," *Proceedings of the 5th Int. Symp. on Long Range Sound Propagation*, Milton Keynes, UK 282–286 (1992).
[38] M. Bérengier, M. Garai, "A state-of-the-art of in situ measurement of the sound absorption coefficient of road pavements," *17th Int. Cong. Acous.*, Rome, Italy (2001).
[39] M. Bérengier, B. Gauvreau, Ph. Blanc-Benon, D. Juvé, "Outdoor sound propagation : a short review on analytical and numerical approaches", Acta Acustica united with Acustica, 89 (6), 980-991, (2003).
[40] Ph. Voisin, Ph. Blanc-Benon, "The influence of meteorological conditions for the localization of an acoustic source by means of a microphone antenna", Acta Acustica united with Acustica, 87, (6) , 695-702, (2001).
[41] T. Van Renterghem, E. Salomons, D. Botteldooren, “Efficient FDTD-PE model for sound propagation in situations with complex obstacles and wind profiles”, Acta Acustica united with Acustica. 91, 671–679, (2005)
[42] D Heimann, R. Karle, “A linearized Euler finite-difference time-domain sound propagation model with terrain-following coordinates”, J. Acoust. Soc. Am. 119, 3813-3821, (2006).